PROCEEDINGS, Thirty-Fifth Workshop on Geothermal Reservoir Engineering
Stanford University, Stanford, California, February 1-3, 2010
SGP-TR-188

# MASSIVELY PARALLEL FULLY COUPLED IMPLICIT MODELING OF COUPLED THERMAL-HYDROLOGICAL-MECHANICAL PROCESSES FOR ENHANCED GEOTHERMAL SYSTEM RESERVOIRS

Robert Podgorney, Hai Huang, and Derek Gaston

Idaho National Laboratory
P.O. Box 1625
Idaho Falls, ID, 83415-3553, U.S.A.
e-mail: Robert.Podgorney@inl.gov

## ABSTRACT

Development of enhanced geothermal systems (EGS) will require creation of a reservoir of sufficient volume to enable commercial-scale heat transfer from the reservoir rocks to the working fluid. A key assumption associated with reservoir creation/stimulation is that sufficient rock volumes can be hydraulically fractured via both tensile and shear failure, and more importantly by reactivation of naturally existing fractures (by shearing), to create the reservoir. The advancement of EGS greatly depends on our understanding of the dynamics of the intimately coupled rock-fracture-fluid-heat system and our ability to reliably predict how reservoirs behave under stimulation and production.

In order to advance our understanding of how reservoirs behave under these conditions, we are developing a physics-based rock deformation and fracture propagation simulator by coupling a discrete element model (DEM) for fracturing with a continuum multiphase flow and heat transport model. In this approach, the continuum flow and heat transport equations are solved on an underlying finite element mesh with evolving porosity and permeability for each element that depends on the local structure of the discrete element network.

This paper describes the first phase of development of the simulator, detailing the development of a parallel, fully coupled, implicit, multiscale geothermal-geomechanical simulation code. The initial code development is being conducted considering only single-phase (water saturated) flow coupled with continuum heat transport and rock mechanics models. DEM and fracture propagating capabilities will be added in the next phase of the code development.

## INTRODUCTION

Reliable reservoir performance predictions of enhanced geothermal reservoir systems require accurate and robust modeling for the coupled thermal-hydrological-mechanical processes. Conventionally, these types of problems are solved using operator splitting methods, usually by coupling a subsurface flow and heat transport simulator with a solid mechanics simulator via input files. One example of such an approach is presented by *Rutquist et al*. (2002), where a widely used flow and heat transport simulator TOUGH2 (*Pruess et al.*, 1999) is coupled to the commercial rock mechanics simulator FLAC (*Itasca Consulting Group*

*Inc*, 1997) via input files. During each time step, TOUGH2 and FLAC run sequentially with the output from one code as input to the other one. Iterations between the codes during each step might be necessary if there is a strong dependence among processes. However, such operator splitting approaches are applicable only to "loosely coupled" problems and usually converge very slowly if at all. For most enhanced geothermal systems, fluid flow, heat transport, and rock deformation are typically strongly nonlinearly coupled.

An alternative is to solve the system of nonlinear partial differential equations that govern fluid flow, heat transport, and solid mechanics simultaneously using a fully coupled solution procedure. This procedure solves for all solution variables (fluid pressure, temperature and rock displacement fields) simultaneously, which leads to one large nonlinear algebraic system that is solved using a strongly convergent nonlinear solver. Developments over the past 10 years in the area of physics-based conditioning, strongly convergent nonlinear solvers (such as Jacobian Free Newton methods) and efficient linear solvers, such as GMRES, make such an approach competitive (*Knoll and Keyes*, 2004).

The overall goal of the project is to develop a parallel physics-based, fully coupled, multiscale modeling tool for predicting the dynamics of fracture stimulation, fluid flow, rock deformation, and heat transport in a single integrated code (i.e., it will eliminate the need for multiple simulations codes to model this tightly coupled process) named FALCON (**F**racturing **A**nd **L**iquid **CON**vection). The code is developed upon a parallel computational framework developed at Idaho National Laboratory (INL) for solving coupled systems of nonlinear equations (*Gaston et al*., 2009), known as MOOSE (**M**ultiphysics **O**bject **O**riented **S**imulation **E**nvironment*)*, which was originally developed for modeling multiphysics problems often encountered in nuclear reactor fuel performance analysis. This computational framework allows for rapid development of multi-dimensional, parallel, implicit, fully coupled, nonlinear simulation capabilities and employs a modular, pluggable architecture that greatly simplifies the process of adding new physical phenomena and coupling of different physics.

As a first step in the development of the code, governing equations for single-phase flow and transport of heat are being coupled with linear elastic equations. The basic architecture of the code allow convenient coupling of different processes and incorporation of new physics , such as stress dependent permeability-porosity, phase change, implicit fracturing and so on without the added difficulty. The following sections present the governing equations used to describe coupled fluid flow, heat transport, and rock mechanics; briefly describe numerical methods, focusing on the Jacobian Free Newton Krylov nonlinear solver; and present a number of simulation results for problems of different level of complexities, followed by discussions and concluding remarks.

## MATHEMATICAL MODELS AND GOVERNING EQUATIONS

Mathematical models describing geothermal systems and geomechanics can be found in the literature. This section will only briefly summarize the derivations described in detail in the literature for geothermal systems (e.g., *Faust and Mercer* 1979a,b; *Brownell, et al*., 1977) and geomechanics (see *Jaeger at al*, 2007). Here, we will focus our discussion on the unique aspects of coupling the governing equations for fully coupled implicit solutions.

The following subsections briefly present conservation equations for the mass, momentum, and energy.

**Fluid Mass Balance**

The mass balance for the fluid may be written as:

$$\frac{\partial(\phi\rho_w)}{\partial t} + \nabla\cdot(\rho_w \mathbf{u_w}) - \acute{q_w} = 0 \tag{1}$$

where $\nabla$ is the vector differential operator. $\boldsymbol{u}_w$ is the flux vector, while $\rho_w$ is the density of the fluid, respectively. $\varphi$ is the porosity of the reservoir.

**Fluid Momentum Balance**

We assume that Darcy's Law is valid. Thus the momentum balance for the fluid is described as:

$$\mathbf{u_w} = \frac{k}{\mu_w}\cdot(\nabla p_w \quad \rho_w g \nabla z) \tag{2}$$

where $k$ is the intrinsic permeability of the reservoir, $\mu_w$ is the viscosity of the fluid, $g$ is the acceleration due to gravity, and $\nabla z$ is a vector of components (0,0,1) when gravity is taken to be aligned in the negative vertical direction.

**Energy Balance**

The energy balance in the system can be described as follows:

$$\begin{aligned}\frac{\partial\left[\phi\rho_w h_w\right]}{\partial t} &+ \nabla\cdot(\rho_w h_w \mathbf{u_w}) + \nabla\cdot\lambda_{cw} \\ &+ \nabla\cdot\lambda_{dw} - \frac{\partial(\phi p_w)}{\partial t} \\ &- \mathbf{u_w}\nabla p_w - \acute{q_w}\acute{h_w} = 0\end{aligned} \tag{3}$$

for the fluid phase and

$$\frac{\partial\left[(1-\phi)\rho_r h_r\right]}{\partial t} + \nabla\cdot\lambda_{cr} = 0 \tag{4}$$

for the reservoir rock matrix, where $h$ is the specific enthalpy, $\lambda_c$ is the heat conduction vector, and $\lambda_d$ is the dispersion vector. Accented terms represent sources and/or sinks in Eqns. 3 and 4.

**Constitutive Relations**

For our simplified single-phase system (water is the model fluid in this paper), constitutive relations are being used to describe the fluid density and viscosity dependence on the temperature.

The density dependence on temperature is described by *Graf* (2009)

$$\begin{aligned}\rho_w = 1000\cdot\Bigg[1 &- \frac{(T-3.9863)^2}{508929.2} \\ &\cdot\frac{T+288.9414}{T+68.12963}\Bigg]\end{aligned} \tag{5}$$

where $T$ is the temperature in degrees Celsius.

Fluid viscosity is represented by the following set of equations, also presented by *Graf* (2009)

$$\mu_w = \begin{cases} 1.787\times10^{-3}\cdot\exp\left[\left(-0.03288 \right.\right. \\ \quad \left.\left. +1.962\times10^{-4}\cdot T\right)\cdot T\right] \\ 10^{-3}\cdot\left[1+0.015512 \right. \\ \quad \left.\cdot\left(T-20\right)\right]^{-1.572} \\ \left(0.2414\times \right. \\ \quad \left. 10^{(247.8/(T+133.15))}\right)\cdot10^{-4} \end{cases}$$

$$for \begin{cases} 0^oC \le T \le 40^oC \\ 40^oC < T \le 10^oC \\ 100^oC < T \le 300^oC \end{cases} \tag{6}$$

## THREE DIMENSIONAL EQUATIONS

Combining Eqns. 1 and 2 yields the following for single-phase flow of water in a deformable, compressible geologic medium.

$$\frac{\partial(\phi\rho_w)}{\partial t} = \nabla \cdot \left[ \frac{k\rho_w}{\mu} (\nabla p - \rho_w g \nabla z) \right] \tag{7}$$

In keeping with our objective of developing a simplified first version of the simulation code, the *Broussinesq Approximation* (*Garg and Kassoy*, 1981) and thermal equilibrium assumption between fluid and rock were used when combining Eqn. 7 with Eqn. 3, to arrive at the following to describe the transport of heat in the system.

$$\left[\phi\rho_w c_w + ((1-\phi)\rho_r c_r)\right]\frac{\partial T}{\partial t} - \nabla\cdot(K_m \nabla T) + \rho_w c_w \mathbf{u_w} \nabla T = 0 \tag{8}$$

where $c_w$ and $c_r$ are the specific heat capacities of the water and rock phases, respectively, and $K_m$ is the medium average thermal conductivity.

Geomechanics of the system is described as follows (*Jaeger et al*, 2007)

$$\rho\frac{\partial^2 u}{\partial t^2} - \nabla\cdot\sigma - \rho\vec{g} - \alpha\nabla p - \beta K \nabla T = 0 \tag{9}$$

where $\boldsymbol{u}$ is the displacement vector; $\alpha$ is the biot effective stress coefficient and $\beta$ is the thermal expansion coefficient. Eq. (9) provides stress equilibrium for a coupled hydro-thermal-mechanical problem.

## NUMERICAL METHODOLOGY

### MOOSE

FALCON has been developed using the MOOSE library (*Gaston et al.*, 2009). This framework provides a strong numerical foundation for rapid development of multi-dimensional, parallel, implicit, fully coupled, nonlinear simulation capabilities. MOOSE is based on a finite element discretization strategy and utilizes state of the art preconditioned Jacobian-Free Newton-Krylov solution methods.

Among the many capabilities MOOSE provides, FALCON makes direct use of the following:

- Flexible, modular systems for defining physics, material properties, boundary conditions, etc.
- Physics based preconditioning.
- Unstructured grid with many element types.
- Hybrid parallelism (threading and MPI) that scales.
- Error estimation.
- Adaptive mesh refinement/ coarsening.
- Ability to read and write numerous solution formats for pre- and post-analysis.

MOOSE itself is based on libMesh a finite element library developed at the University of Texas in Austin. (*Kirk et al.*, 2006)

### Finite Element Discretization

MOOSE utilizes a Galerkin finite element based solution method. Finite element schemes are a subset of the method of weighted residuals in which a particular function space is chosen to represent both the function to solve for and the function to weight against. The input that must be supplied for this method is what's known as the "weak form" of partial differential equations. Weak forms are generated by multiplying a PDE by a weighting function (also called a "test function" that we denote $\phi_i$) and then integrating over the domain. Further manipulation is often necessary to reduce the order of derivatives present in the problem, allowing more flexibility in the

choice of function space used to represent the solution and the test function.

Taking the flow equation defined above (Eqn. 7), multiplying by $\phi_i$, integrating over the domain (denoted by "(,)"), applying the Gauss divergence theorem to reduce the derivative order of the equation (generating a boundary integral denoted by "<,>") and setting the it equal to zero the following weak form is found:

$$\begin{aligned}
&\left(c_f \rho_w \phi P_t, \phi_i\right) \\
&\quad + \left(\frac{k\rho_w}{\mu_w} \cdot \nabla p, \nabla \phi_i\right) \\
&\quad - \left\langle \frac{k\rho_w}{\mu_w} \cdot \nabla p \cdot \mathbf{n}, \phi_i \right\rangle \\
&\quad + \left(\frac{k\rho_w}{\mu_w} \cdot \nabla \rho_w g \nabla z, \nabla \phi_i\right) \\
&\quad - \left\langle \frac{k\rho_w}{\mu_w} \cdot \nabla \rho_w g \nabla z \cdot \mathbf{n}, \phi_i \right\rangle = 0
\end{aligned} \tag{10}$$

Applying a similar process to Eqns. 8, 9 we can find the weak forms:

$$\begin{aligned}
&\left(T_t\left[\phi\rho_w c_c + (1-\phi)\rho_r c_r\right], \phi_i\right) \\
&\quad + \left(\rho_w c_w \mathbf{u_w} \nabla T, \phi_i\right) \\
&\quad + \left(K_m \nabla T, \nabla \phi_i\right) \\
&\quad - \left\langle K_m \nabla T \cdot \mathbf{n}, \phi_i \right\rangle - 0
\end{aligned} \tag{11}$$

$$\begin{aligned}
(\rho u, \phi_i) - &((\sigma_{xx}, \sigma_{yx}, \sigma_{zx}, \nabla\phi_i) \\
&-(\rho g_x, \phi_i) - (\alpha \partial P/\partial x, \phi_i) \\
&-(3\beta K \partial T/\partial x, \phi_i) = 0 \\
(\rho v, \phi_i) - &((\sigma_{xy}, \sigma_{yy}, \sigma_{zy}, \nabla\phi_i) \\
&-(\rho g_y, \phi_i) - (\alpha \partial P/\partial y, \phi_i) \\
&-(3\beta K \partial T/\partial y, \phi_i) = 0 \\
(\rho w, \phi_i) - &((\sigma_{xz}, \sigma_{yz}, \sigma_{zz}, \nabla\phi_i) \\
&-(\rho g_z, \phi_i) - (\alpha \partial P/\partial z, \phi_i) \\
&-(3\beta K \partial T/\partial z, \phi_i) = 0
\end{aligned} \tag{12}$$

where *u*, *v* and *w* are component variables of the displacement vector.

**Jacobian-Free Newton-Krylov**

The previous section developed a set of discretized, coupled, nonlinear weak form equations. FALCON, through MOOSE, utilizes a Newton solution method for this system of equations that endeavors to solve for:

$$\mathbf{F}(\mathbf{U}) = 0, \tag{13}$$

where F() represents the residual and U is the full solution vector U ={*P*, *T*, *u*, *v*, *w*}$_T$. Note that this is a fully-coupled scheme, simultaneously reducing the non-linear residual for all solution variables. Application of Newton's method to the discretized form of the equations naturally leads to a linear algebraic system to solve for each Newton iteration:

$$\mathbb{J}\delta\mathbf{U}^k = -\mathbf{F}(\mathbf{U}^k), \tag{14}$$

where *k* denotes the iteration number, δU is the Newton update to solve for and J is the Jacobian matrix:

$$\mathbb{J}(\mathbf{U}) = \frac{\partial \mathbf{F}_i(\mathbf{U})}{\partial \mathbf{U}_j}, \tag{15}$$

i.e., the partial derivative of each residual (*i*) with respect to each solution variable (*j*).

After Eq. 14 has been solved for $\delta U_k$, U is then updated by:

$$\mathbf{U}^{k+1} = \mathbf{U}^k + \delta\mathbf{U}^k. \quad (16)$$

The new iterate ($U_{k+1}$) is then used in Eq. 14 and the process starts over again until $F(U_{k+1})$ is within a specified tolerance of zero. Typically a tolerance such as $10^{-8}$ is sufficient.

The solution of the linear system in Eq. 14 is, in this work, found using a Krylov method (such as GMRES). This forms a Newton-Krylov method, where the inner linear systems are approximately solved (within a tolerance) using a Krylov method. Efficient solution of linear systems using Krylov methods demands the development of an effective preconditioner, which we will describe in the following section.

Often it is the case that the Jacobian matrix (Eq. 15) is expensive to form, requires a large amount of memory to store and is difficult to find (due to the need to calculate analytic derivatives). In part because of these concerns, the present work utilizes the Jacobian-Free-Newton-Krylov (JFNK) method (*Brown and Saad*, 1990; *Knoll and Keyes*, 2004). JFNK alleviates the need to form Jacobian (Eq. 15) by recognizing that Krylov methods work through the repeated application of Jacobian-vector products and never utilize the Jacobian by itself. The action of the Jacobian in a Krylov method can be approximated using the finite difference form:

$$\mathbb{J}\mathbf{v} \approx \frac{\mathbf{F}(\mathbf{U} + h\mathbf{v}) - \mathbf{F}(\mathbf{U})}{h}, \quad (17)$$

where *h* is a perturbation parameter and *v* is provided by the Krylov method. Several methods exist for computing *h*, but in general, it is chosen to avoid problems with machine precision.

**Preconditioning**

Utilizing Eq. 17, Eq. 14 can now be solved without the need to develop both the mathematical expressions for the true Jacobian or fill the Jacobian matrix; the former saving development effort and the latter execution time. However, execution speedup is not guaranteed. The computational burden has now shifted from Jacobian formation to residual computation. In a Krylov solver, Eq. 17 must be evaluated during each linear iteration. If a large number of linear iterations are necessary to solve Eq. 14 this burden might overshadow Jacobian formation and inversion. To combat this, preconditioning must be applied.

Preconditioning attempts to lower the condition number of a linear system, making it more amiable to solution using iterative methods such as a Krylov method. In the present work right preconditioning is employed, augmenting Eqs. 14 and 17:

$$\mathbb{J}P^{-1}(P\delta\mathbf{U}^k) = -\mathbf{F}(\mathbf{U}^k), \quad (18)$$

$$\mathbb{J}P^{-1}\mathbf{v} \approx \frac{\mathbf{F}(\mathbf{U} + hP^{-1}\mathbf{v}) - \mathbf{F}(\mathbf{U})}{h}, \quad (19)$$

where P represents a preconditioning matrix. Note that if P = J then the system reduces to $I\delta U_k = -F(U_k)$ and is trivial to solve. Unfortunately, this still requires finding $P^{-1} = J^{-1}$, thus nothing has been gained. The idea is to find $P \approx J$ such that $P^{-1}$ is computationally advantageous to find while still significantly improving the conditioning of the system.

One possibility for P is to fill the diagonal blocks with the diagonal blocks of J. This has the effect of developing a matrix that looks like a decoupled Jacobian, capturing a lot of the behavior of the true-coupled

system without all of the complexity. This block diagonal matrix can then be partially inverted using methods like ILU, Jacobi, and multigrid. Multigrid methods, and specifically Algebraic Multigrid (AMG) methods, are particularly interesting because of their ability to provide a good approximation to the inverse of a matrix that is dominated by elliptic looking operators (*Henson and Yang*, 2002). Considering several governing equations include prominent elliptic components the choice of a block diagonal P being partially inverted by AMG was the most frequently used approach for this study.

MOOSE also provides the ability to perform physics-based preconditioning, where each physics is targeted with a different preconditioning method. Physics-based preconditioning allows for more efficient and simultaneously more effective preconditioning. For more information on physics-based preconditioning and its use within the MOOSE framework, see (*Park et al.*, 2010). The use of physics-based preconditioning within FALCON is an ongoing area of research.

## MODEL APPLICATION

### One-dimensional (1D) flow and heat transport, comparison with analytical solution

Our first example is to solve a simple one-dimensional heat conduction-convection problem using FALCON and compare the numerical solution with the analytical solution. In this particular example, only two equations, fluid flow and heat transport, are solved. Furthermore, for simplicity, we assumed constant fluid density and viscosity. Figure 1 shows problem geometry, the mesh used in the simulation and simulation results at three different stages.

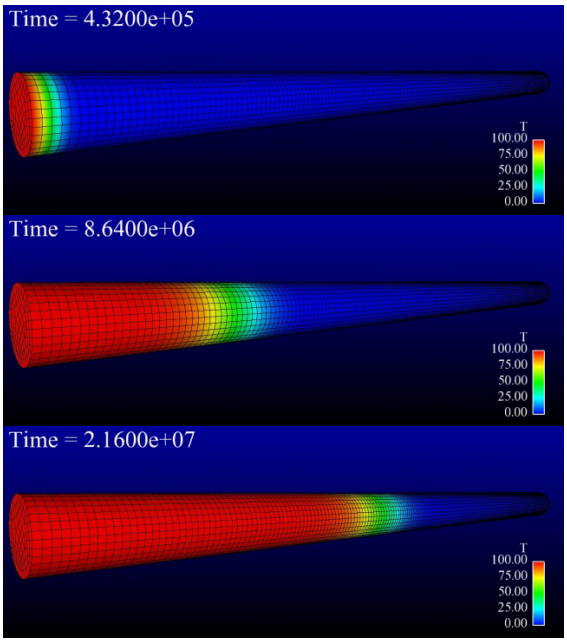


*Figure 1.Three-dimensional mesh for a 1D cylindrical column and simulation results.*

Figure 2 shows the comparison between numerical and analytical solutions at two different times. It is very clear that the numerical solution agrees very well with the analytical solution.

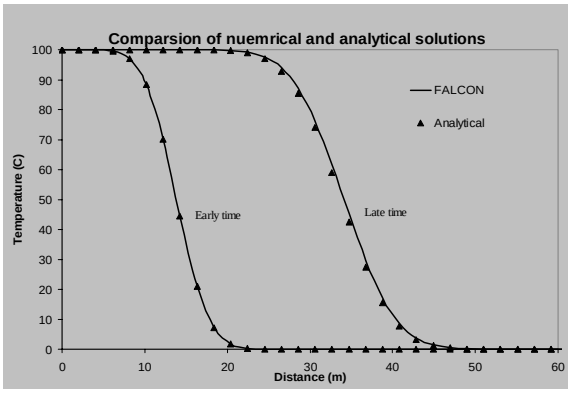


*Figure 2.Comparison of the numerical and analytical solutions for 1D heat conduction-convection problem.*

### Two-Dimensional Thermal Induced Convection and Instability

The second example examines a case of density driven free thermal convection, similar to that detailed by Elder (1967), in which a water saturated homogeneous

isotropic medium is heated from the bottom causing a large density change (>5%) and leads to unstable flow. This example was chosen to demonstrate FALCON's capabilities for fully coupling the fluid flow and heat transport equations along with the temperature-dependent constitutive relations for fluid density and viscosity, as well as adaptive mesh refinement (AMR).

The simulation domain and boundary condition locations chosen for the problem follows those detailed by Oldenberg and Pruess (1995), using symmetry about the midpoint of the x-axis of the Elder problem, reducing the domain size to 300 meters by 150 meters. Initial conditions chosen for the problem are a hydrostatic pressure distribution and a uniform $12^{O}$ C over the entire domain. The bottom left (x = 0 to 150m) boundary condition imposed at startup applies a constant temperature of $20^{0}$C, and initiates a density driven instability into the system. Relevant material properties used in the simulation are an intrinsic permeability of $1x10^{-10}$ $m^2$, porosity of 0.40, rock specific heat of 920.0 J/kg $^{O}$C, and a rock density of 2,500 kg/$m^3$. Fluid density and viscosity are initialized at values provided from the constitutive relations provided above. The problem was specifically parameterized to be convection dominated and have a large Rayleigh number, testing the stability and efficacy of the code.

Oldenberg and Pruess (1995) showed that the results of this problem are strongly grid dependent, with a relatively coarse grid returning [upward] flows concentrated along the axis of symmetry in their simulations. When a finer grid was used an area of downwelling was predicted along the axis of symmetry.

Three simulation cases were tested with FALCON focusing on fine mesh scenarios and adaptive mesh refinement. The cases were 1) a uniform 1m by 1m mesh, 2) a uniform 10m by 10m mesh with aggressive adaptive mesh refinement, and 3) a uniform 10m by 10m mesh with conservative adaptive mesh refinement. Shown on Figure 3 is the temperature distribution after twenty years of simulated time. The red color represents a temperature of $20^{O}$C, whereas the blue color represents $12^{O}$C. The meshes used in the simulations are shown on Figure 4.

As can be seen on Figure 3, the results for the two adaptive mesh simulations return similar results, whereas there is a difference when compared to the static fine mesh simulation. *Frolkovic and DeSchepper* (2000), when comparing the results of fine grid simulations and adaptive mesh applications, reported that adaptive mesh results being identical to those obtained with an extremely fine mesh. While our fine mesh test cases do not directly compare with those of *Frolkovic and DeSchepper* (2000), examination and comparison of the simulation case results are illustrative of the potential gains in computational capability obtained with FALCON.

The first simulation case using a uniform 1m by 1m grid (45,000 grid blocks), shown in the top frame on Figure 3, predicted a large central upwelling zone and three additional upwelling fingers. The 20-year simulation required approximately 2,100 seconds for the calculations using a MPI scheme with 8 processors and a uniform timestep of 10 days. The second and third cases, both using an initial 10m by 10m mesh and adaptive mesh refinement, produced very similar results. For the second (aggressive adaptive mesh refinement) case, the mesh refinement was allowed to reduce the grid cells to 0.15m by 0.15m, and forced the refined areas to persist over a large area of the simulated domain. As the mesh evolved over the duration of the simulation, the simulation time actually suffer when

compared to the uniform mesh case, requiring a total of 4,077 seconds to simulate 20 years of convection. The aggressive mesh refinement resulted in the existence of 37,047 grid cells at the conclusion of the simulation. The third test case produced similar results as the second case (see Figure 3), but with much less computational burden. Allowing the grid only to refine to a uniform 1.25m cell size, and relaxing the grid after perturbations passed by, reduced the computational time to 434 seconds to complete the simulation. 5,826 grid cells existed at the conclusion of the run.

While our results are preliminary and qualitative in nature, they are very promising. Significant reductions in computational time were achieved using adaptive meshing capabilities. Questions remain however, regarding quantification of the simulation results and predicted temperature distribution. Work is currently ongoing to quantify the solution of the problems and benchmark the code performance against existing simulators.

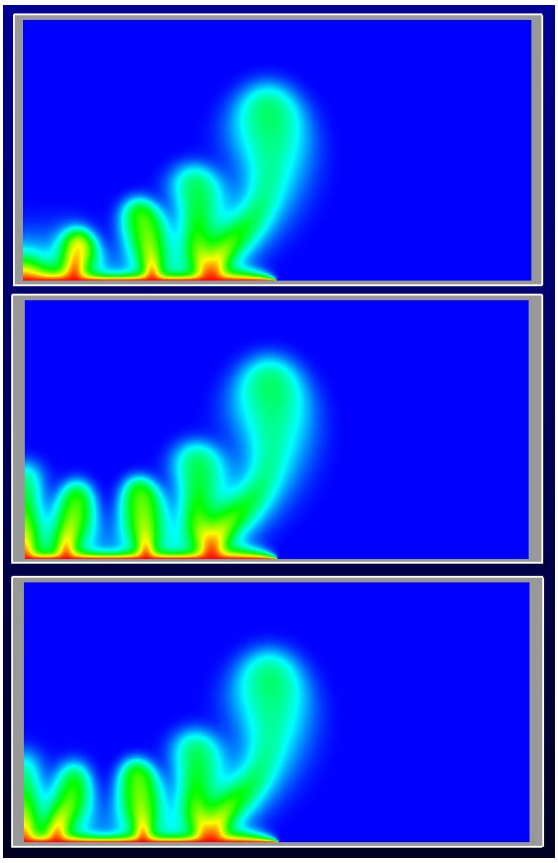

*Figure 3.Simulated temperature distribution for unstable thermal convection using a fixed mesh (top), aggressive adaptive mesh (middle), and conservative adaptive mesh (bottom).*

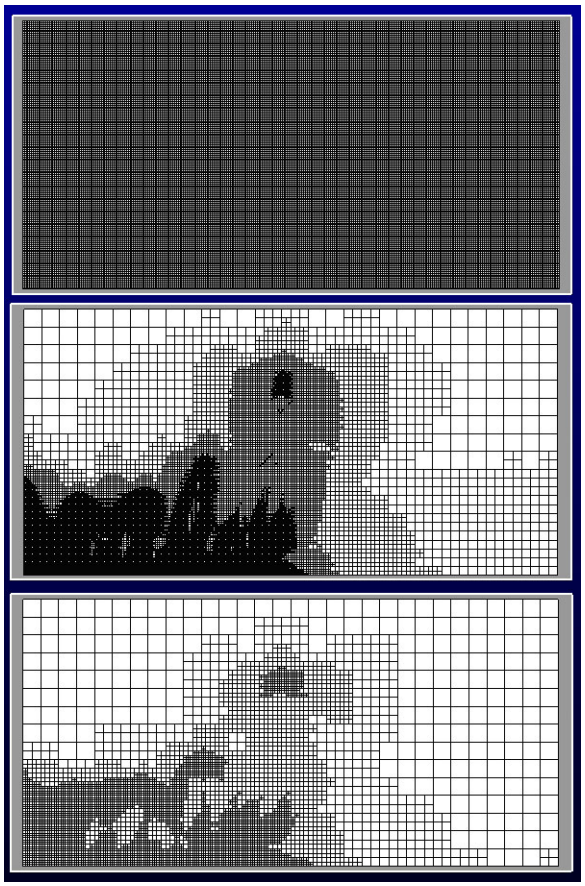

*Figure 4. Mesh corresponding to simulation cases shown in Figure 3.*

## Three-Dimensional Wellbore-scale Coupled Thermal-Hydro-Mechanical Problems

Here we consider modeling a more complex coupled thermoporoelastic problem in the vicinity of injection well due to injection of cold water into an initially hot reservoir in order to demonstrate the capability of our fully coupled modeling approach. Firstly, we consider only fluid-rock interaction and ignore the thermal-induced rock deformation effect (a classical poroelasticity problem). Figure 5 shows the problem geometry and finite element mesh used in this simulation. Both lateral and bottom boundaries are confined (with prescribed zero lateral displacement).

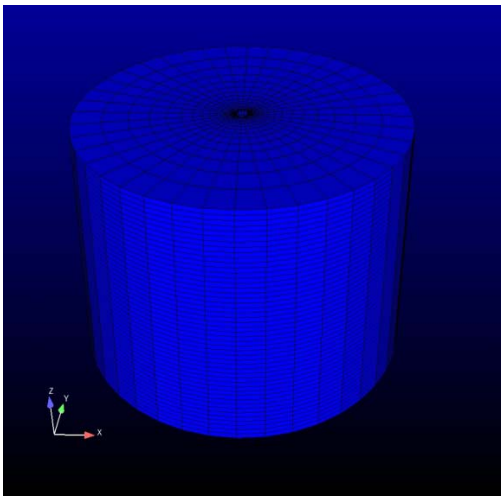

*Figure 5. Three-dimensional mesh in the vicinity of an injection well. Notice that in this problem, the wellbore is explicitly meshed.*

Water is injected via the injection well in the middle of the domain at a constant rate. Figure 6 shows the simulation results of the final steady-state 3D pressure and rock displacement fields. The simulation results clearly show the coupling of fluid injection and rock deformation and are qualitatively reasonable. The rock bulging out across the top surface due to the lateral confinement boundary condition used in this simulation. This is very similar to thermal expansion near a heater well. Readers also need to notice that the vertical displacement has been largely exaggerated in order to visualize the bulging effect. The actual vertical and lateral displacements are indeed very small. The lateral displacement field indicates that the rock is “pushed” away from the injection well, also a clear evidence of fluid-rock interaction. Also notice that in this simulation, only fluid to rock displacement is modeled for simplicity. The effect of rock deformation on fluid flow can be easily incorporated into the simulation.

A more complex problem is to add heat transport and couple all three processes—fluid flow, heat transport, and rock deformation due to both fluid injection and

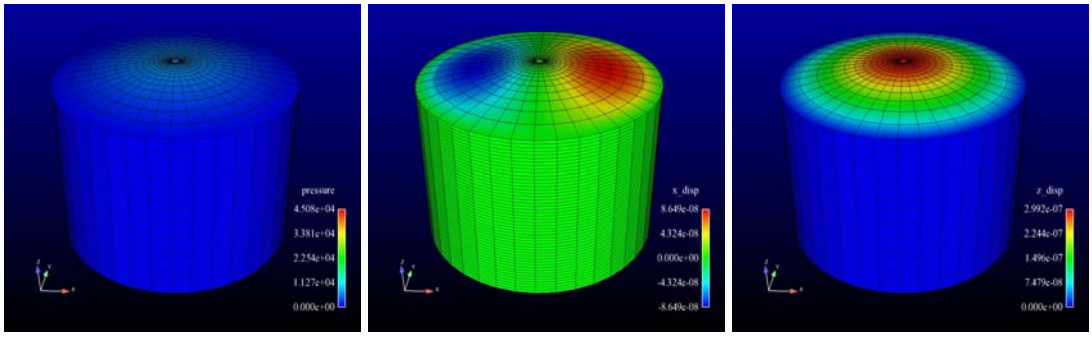


*Figure 6. Simulation results of the poroelastic problem-steady-state solution: (left) pressure field in Pascal; (mid) lateral (x-component) displacement field in meters and (right) vertical (z-component) displacement field in meters. Note that displacement fields are exaggerated for visualization purpose.*

thermal-induced stress—together by solving all three governing equations (Eqns. 7-9) simultaneously. Figure 7 shows the simulation results for such a problem. In this simulation, cold water at 20°C is injected into the reservoir that is initially at a temperature of 100°C, which leads to decreasing reservoir temperature (as shown in Figure 7). Therefore the rock near the wellbore tends to shrink toward the injection well due to cooling, a processes similar to land subsidence due to excessive groundwater pumping. A close comparison between Figures 6 and 7 on the magnitudes and displacement directions for the lateral and vertical displacements indicates that in this particular example, the deformation of rock due to reservoir cooling is far more significant that that due to injection of water. Thus the rock near the wellbore is under tension. One immediate application of the simulation results is to evaluate the stress state near the wellbore and potential of rock failure.

## DISCUSSION AND CONCLUSIONS

Commercial scale deployment of EGS greatly depends on our understanding of the dynamics of the coupled rock-fracture-fluid-heat system and our ability to reliably predict how reservoirs behave under stimulation and production. A key assumption associated with reservoir creation is that the reservoir rock can be hydraulically fractured in quantities sufficient to allow for commercial levels of heat transfer.

The work detailed in the paper documented the development of a parallel, fully coupled, implicit, multiscale geothermal-geomechanical simulation code. While this is just the initial code development, focusing only on a single-phase, continuum based description of the processes, further work is underway to extend the processes described to multiphase flow and couple the continuum mechanical equations with mesos-scale DEM descriptions of rock failure and fracture propagation.

The framework developed for the code to date provides a strong numerical foundation for further development of more complex problems, utilizing the MOOSE library for a finite element discretization strategy and state of the art preconditioned Jacobian-Free Newton-Krylov solution methods and multiscale coupling .

Testing the code against a one-dimensional analytical solution for single-phase flow and heat transport in porous media showed that

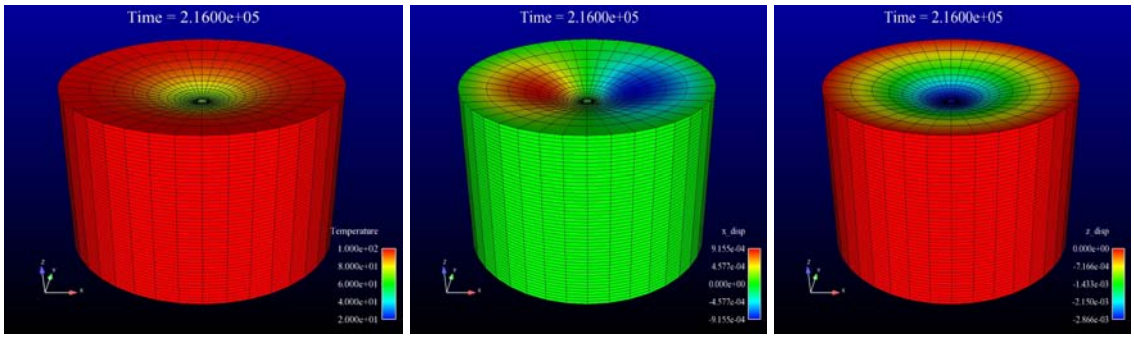


*Figure 7. Simulation results of the thermoporoelastic problem- solution after two days of injection of cold water into a hot reservoir: (left) temperature field in °C; (mid) lateral (x-component) displacement field in meters and (right) vertical (z-component) displacement field in meters.*

the predicted temperatures agreed very well with the analytical solution. Testing a more challenging, two-dimensional fully coupled example, similar to that described by Elder (1967), demonstrated the adaptive mesh capabilities of the code. While the two-dimensional results are preliminary and qualitative in nature, they are very promising. Significant reductions in computational time were achieved using adaptive meshing capabilities. Questions do remain however, especially regarding grid sensitivity and the effect of adaptive meshing schemes on predicted temperature distributions. These topics have been the focus of significant research in the past, and are a fertile area for future work.

Simulation of coupled thermoporoelastic processes in the vicinity of injection well due to injection of cold water into an initially hot reservoir demonstrated the capability of our fully coupled modeling approach. Two cases were examined, 1) a classical poroelasticity problem which considered only fluid-rock interactions, and 2) a fully coupled case where fluid flow, heat transport, and rock deformation due to both fluid injection and thermal-induced stress (coupling all three governing equations), were solved simultaneously. The magnitudes and displacement directions predicted for this example are reasonable and qualitatively agree with many previous studies. The preliminary results clearly demonstrate the potential of applying physics-based, fully coupled numerical models to advance the understandings of strongly nonlinear, tightly coupled thermal-hydro-mechanical processes that are extremely difficult to study via physical experiments.

## ACKNOWLEDGEMENTS

The work described in this paper was supported by the U.S. Department of Energy, Assistant Secretary for Energy Efficiency and Renewable Energy (EE), under DOE Idaho Operations Office Contract DE-AC07-05ID14517.

## REFERENCES

Brown, P. N. and Y. Saad (1990). Hybrid Krylov methods for nonlinear systems of equations. SIAM J. Sci. Statist. Comput. 11(3), 450–481.

Brownell, D., S. Garg, and J. Pritchett (1977). Governing equations for geothermal reservoirs. Water Resources Research 13(6), 929–934.

Elder, J. (1967). Transient convection in a porous medium. JOURNAL OF FLUID MECHANICS 27(Part 3), 609

Faust, C. and J. Mercer (1979a). Geothermal reservoir simulation .1. Mathematical-models for liquid- dominated and vapor-dominated hydrothermal systems. WATER RESOURCES RESEARCH 15(1), 23–30.

Faust, C. and J. Mercer (1979b). Geothermal reservoir simulation .2. Numerical-solution techniques for liquid-dominated and vapor-dominated hydrothermal systems. WATER RESOURCES RESEARCH 15(1), 31–46.

Frolkovic, P. and H. De Schepper (2000). Numerical modeling of convection dominated transport coupled with density driven flow in porous media. ADVANCES IN WATER RESOURCES 24(1), 63–72.

Garg S. and D. Kassoy (1981). Convective heat and mass transfer in hydrothermal systems, *in* L. Rybach and L. Muffler, eds. Geothermal Systems: Principles and Case Histories. Wiley.

Gaston, D., C. Newman, G. Hansen, and D. Lebrun-Grandi´e (2009). MOOSE: A parallel computational framework for coupled systems of nonlinear equations. Nucl. Engrg. Design 239, 1768–1778.

Graf, T. (2009). Simulation of geothermal flow in deep sedimentary basins in Alberta. ERCB/AGC Open File Report 2009-11.

Henson, V. E. and U. M. Yang (2002) BoomerAMG: A parallel algebraic multigrid solver and preconditioner. Appl. Numer. Math. 41:155–177.

Itasca Consulting Group. (1997). *FLAC 3D, Fast Lagrangian Analysis of Continua in 3 Dimensions. Version 2.0.* Five volumes. Minneapolis, Minnesota, Itasca Consulting Group.

Jaeger, J.C., N.G.W. Cook, and R.W. Zimmerman. (2007). Fundamentals of rock mechanics, 4th ed., Blackwell.

Knoll, D. A. and D. E. Keyes (2004). Jacobian-free Newton- Krylov methods: a survey of approaches and applications. J. Comput. Phys. 193(2), 357–397.

Kirk, B.S., J. W. Peterson, R. H. Stogner, and G. F. Carey (2006). . libMesh: a C++ library for parallel adaptive mesh refinement/coarsening simulations. Eng Comput-Germany, 22(3-4):237–254

Mercer, J. and C. Faust (1979). Geothermal reservoir simulation .3. Application of liquid-dominated and vapor-dominated hydrothermal modeling techniques to Wairakei, New Zealand. WATER RESOURCES RESEARCH 15(3), 653–671.

Oldenburg, C. and K. Pruess (1995). Dispersive transport dynamics in a strongly coupled groundwater-brine flow system. WATER RESOURCES RESEARCH 31(2), 289–302.

Park, H., D. A. Knoll, D.R. Gaston, and R.C. Martineau (2010) Tightly coupled multiphysics al- gorithms for pebble bed reactors. Nuclear Science and Engineering, *in review*.

Pruess, K., C. Oldenburg, G. Moridis. (1999). TOUGH2 User's Guide, Version 2.0, Report LBNL-43134. Lawrence Berkeley National Laboratory, Berkeley, CA.

Rutqvist, J., Y.-S. Wu, C.-F. Tsang and G. Bodvarsson (2002), A modeling approach for analysis of coupled multiphase fluid flow, heat transfer, and deformation in fractured porous rock. *Int. J. Rock Mech. Min. Sc.i.* 39, 429–442